Prediction of in-plane stiffness properties of Non-Crimp Fabric laminates by means of 3D Finite Element analysis

Authors: Amparo González, Enrique Graciani (corresponding author), Federico París.

Affiliation (for all authors): Grupo de Elasticidad y Resistencia de Materiales, Escuela Superior de Ingenieros, Universidad de Sevilla.

Address (for all authors):

Address: Grupo de Elasticidad y Resistencia de Materiales.
Escuela Superior de Ingenieros, Universidad de Sevilla.
Camino de los Descubrimientos s/n.
41092 Sevilla, España.

Phone: +34 954 487 300 Fax: +34 954 461 637

E-mail: graciani@esi.us.es (Enrique Graciani), paris@esi.us.es (Federico París).

Abstract

Non-crimp fabric (NCF) composites are constituted by differently oriented layers of ideally unidirectional fibre tows. However, a slight waviness always appears in the tows. The applicability of the General Laminate Theory (GLT) to obtain the stiffness properties of NCF laminates is elucidated in this paper. For this purpose, a 3D finite element (FE) model of the representative unit cell (RUC) of a single NCF lamina has been carried out to obtain its apparent stiffness properties, which are employed, along with the GLT, to determine the stiffness properties of the laminate. These properties are compared with those obtained from the FE model of the RUC of the whole laminate for several configurations with different stacking sequences, fibre contents and crimp angles. Finally, predictions are compared with existing experimental results. The numerical results achieved validate the use of the GLT in NCF composites, once the lamina properties have been calculated taking into account the internal structure of these materials.

Keywords

A. Fabrics/textiles; A. Polymer-matrix composites (PMCs); B. Mechanical properties; B. Modelling; C. Finite element analysis (FEA).

1.- Introduction

Composites offer considerable advantages in low weight components needing high strength and stiffness due to their high specific mechanical properties. Nevertheless, their high manufacturing cost as well as their poor behaviour under out-of-plane loads have limited their use in many cases to secondary structures. In response to this fact, new types of composites are being developed, the material considered in this study, non-crimp fabric (NCF) composites, being one of them [1].

Essentially, the structure of this type of material consists of a set of laminas of ideally parallel tows, which are constituted by a large amount of fibres placed side by side and stitched together. All the tows of one lamina have their fibres oriented along the same direction but the orientation of the laminas may be different as in classical composites made from pre-pregs. Manufacturing is usually carried out by out-of-autoclave liquid resin infusion techniques, ensuring that the resin impregnates the fibres inside the tows and fills the channels between them. The compaction during the processing forces the tows to curve into the adjacent resin pockets, acquiring a slightly wavy shape. As a consequence, NCF laminates have a complicated and irregular internal architecture, heterogeneous not only at micro-scale but also at meso-scale, see Fig. 1, which may affect their mechanical performance under loading.

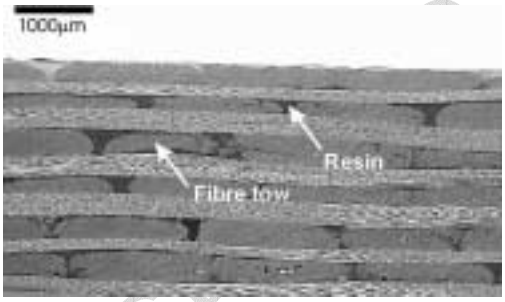

Figure 1. Cross-section of a typical NCF composite [2].

In relation to traditional composites, NCF laminates are in an intermediate position between pre-preg laminates and conventional fabrics (see Ávila [3] for a comprehensive literature review on NCF composites). The better strength of NCF laminates under out-of-plane loads, if compared with pre-preg laminates, is due to the stitching of the tows. The better in-plane properties, if compared with conventional woven fabrics, are due to the fact that NCF laminates have less fibre waviness than woven composites.

As dry fabrics are employed, the use of technologies derived from the textile industry and the fact that there is no risk of polymerization during storage reduces the manufacturing cost of NCF pieces. In contrast, the stitching which is being employed nowadays has proved not to be stiff enough to guarantee the correct alignment of the tows during manufacturing, which may lead to non homogeneous distribution of the properties in the final laminates.

As a consequence of the irregular internal architecture of the NCF laminates, the Finite Element (FE) analysis of a certain component made of these materials becomes a significantly complicated task. The difficulties in the FE analysis arise both in the preprocessing and the postprocessing stage. Firstly, in the preprocessing stage, averaged stiffness properties of the NCF laminates are needed to allow the use of standard shell elements in the modelling of the NCF components, and, secondly, once the averaged strains and stresses at each point of the component are obtained from the numerical analysis, a specific failure criterion is needed to decide if these strains and stresses are allowable or will cause breakage of the laminate (or will create some damage, reducing its apparent stiffness properties).

As can be seen from the works of Drapier and Wisnom [4-5], in which a 2D FE model of a typical NCF laminate is studied under shear and compressive loads, these difficulties can be addressed using a FE model of the representative unit cell of the laminate carried out at mesomechanical level.

The work presented in this paper is dedicated to the numerical estimation of the in-plane stiffness properties of several laminates of this material, using FE models elaborated at mesomechanical level. The use of these mesomechanical FE models of NCF materials to develop specific failure criteria will be presented in future publications.

The present work has been carried out within the framework of the project FALCOM "Failure, Performance and Processing Prediction for Enhanced Design with Non-Crimp-Fabrics Composite", financed by The European Union (under EC contract No. G4RD-CT-00694). This Project has given rise to different publications, those appearing in [1,5-8] being the closest to the present paper. Biaxial laminates, using combinations of [0,90] lay-ups, are employed in this paper for the characterization of NCF laminates because they were selected within the FALCOM project as the object of study.

As has been mentioned above, in the present study NCF composites have been analyzed at mesomechanical level. At this level, they can be considered as constituted by homogenous tows and resin

pockets that fill the gaps left between them. As can be appreciated in Fig. 1, the internal structure at this level is highly complicated. As a consequence of this, it is difficult to develop FE models that reproduce this internal structure, especially when the tows in consecutive laminas are not forming right angles. Therefore, it is interesting to find numerical procedures to predict the apparent in-plane stiffness properties of NCF laminates without modelling the whole thickness of the laminate.

A numerical procedure, in which only a representative 3D unit cell of a single NCF lamina must be modelled, has been employed in the present study. In this procedure, the apparent stiffness properties of differently oriented laminas inside the laminates are evaluated using the developed FE model of a single NCF lamina. Subsequently, these properties are used to calculate the stiffness properties of the laminates applying the General Laminate Theory. To validate the previous procedure, FE models of the representative unit cell of whole laminates, with different combinations of [0,90] lay-ups, have been made and the results obtained with both procedures having been compared.

Once the validity of the General Laminate Theory has been stated for NCF laminates, a parametric numerical analysis has been carried out to study the influence of certain material parameters in their apparent stiffness. In particular, the analysis has been focused on determining the influence that the internal architecture of the material and the stiffness properties of the constituents, tows and resin, may have in the apparent stiffness of the NCF laminas and laminates.

Finally, a comparison with the experimental results obtained within the FALCOM project has also been carried out, showing a reasonably good agreement.

2.- Evaluation of the stiffness properties of NCF laminates

Two alternative procedures have been considered in the present study to estimate numerically the apparent stiffness properties of several NCF laminates. The first procedure, which will be named "Lamina Numerical Model" (LaNM in the following), employs a 3D FE model of a representative unit cell of a single NCF lamina to obtain the apparent stiffness properties of the lamina, and evaluates the apparent stiffness properties of a particular NCF laminate making use of the General Laminate Theory. The second procedure, which will be referred to as "Laminate Numerical Model" (LeNM in the following), employs a 3D FE model of a representative unit cell of the full laminate and its apparent stiffness properties are directly obtained from this model applying an appropriate set of boundary conditions.

Both procedures have been employed to predict the apparent stiffness properties of $[0,90]_2$ and $[0,90]_s$ laminates. The global coordinate systems employed to define the laminates are parallel to the orthotropic directions of the abovementioned laminates. The stiffness properties calculated from the LaNM correspond to the 0º laminas of the laminates. The stiffness properties of each particular lamina are defined by the following relationship: $\boldsymbol{\sigma}^k = \boldsymbol{Q}^k \boldsymbol{\varepsilon}^k$, which can be written in full as:

$$\begin{pmatrix} \sigma_{11}^k \\ \sigma_{22}^k \\ \sigma_{12}^k \end{pmatrix} = \begin{pmatrix} Q_{11}^k & Q_{12}^k & 0 \\ Q_{12}^k & Q_{22}^k & 0 \\ 0 & 0 & Q_{66}^k \end{pmatrix} \begin{pmatrix} \varepsilon_{11}^k \\ \varepsilon_{22}^k \\ \gamma_{12}^k \end{pmatrix} \tag{1}$$

where the superscript k denotes the position of the lamina inside the laminate. The global coordinate system is employed in this equation, '1' being the longitudinal direction of the tows in the 0º laminas, '2' being the longitudinal direction of the tows in the 90º laminas and '3' being the thickness direction of the laminate.

Assuming that all the laminas of the laminates considered have similar geometrical characteristics and stiffness properties in their orthotropic axis, the stiffness properties of the 90º laminas in the global axis of the laminates can be calculated from the stiffness properties of the 0º laminas, using:

$$Q_{11}^{90^\circ} = Q_{22}^{0^\circ},\ Q_{22}^{90^\circ} = Q_{11}^{0^\circ},\ Q_{12}^{90^\circ} = Q_{12}^{0^\circ} \text{ and } Q_{66}^{90^\circ} = Q_{66}^{0^\circ} \tag{2}$$

The apparent stiffness matrix of the laminates is calculated by applying:

$$Q_{ij} = \frac{1}{N} \sum_{k=1}^{N} [Q_{ij}^k t^k] \tag{3}$$

where, t^k is the thickness of lamina k, N is the number of laminas and Q_{ij} represents the components of the stiffness matrix of the laminate.

Finally, the apparent in-plane elasticity moduli, $E_{11} = E_{22}$, the apparent in-plane Poisson ratio ν_{12} and the apparent in-plane shear modulus G_{12} of each laminate can be calculated from its stiffness matrix using:

$$E_{11} = E_{22} = Q_{11}\left(1 - \frac{Q_{12}^2}{Q_{11} Q_{22}}\right),\ \nu_{12} = \frac{Q_{12}}{Q_{22}},\ G_{12} = Q_{66} \tag{4}$$

Note that, in the LaNM approach, the use of (1)-(4) allows the stiffness properties of an NCF laminate to be evaluated using only the FE model of a representative unit cell of a single lamina of this material. This is a great advantage when dealing with laminates that have laminas oriented in directions other than 0º and 90º, in which the building of a through thickness FE mesomechanical model is of enormous complexity.

3.- Geometry and boundary conditions of the FE models

The present study has been carried out at mesoscopic scale. For this reason, the NCF laminas have been considered as constituted by tows and resin pockets filling the gaps between them. Stitching of the tows has not been taken into account in the present study, because it only has significant influence on out-of-plane failure properties and consequently its effect on the in-plane stiffness properties can be neglected.

In previous studies, Drapier and Wisnom [4-5] studied the performance and failure of NCF composites using 2D FE models of a representative unit cell of the laminates. In those analyses, the authors assume a generalised plane-strain case to represent the 3D media with 2D FE models and, consequently, it is considered that the internal geometry of the material does not change along the direction perpendicular to the plane of the model (that is, the longitudinal direction of the 90º tows).

Although , as was pointed out by París *et al.* [6], 2D FE models are able to perform representative studies of NCF laminates, as shown in [4-5], the internal architecture of the actual NCF laminates is not completely represented by them, since it is highly irregular along any direction of the material. For this reason, several 3D FE models have been developed in the present study in order to clarify whether the variations of the internal structure of the material, along both in-plane directions, play a role in the performance of the NCF composites. Additionally, the use of these 3D FE models will permit the calculation of the in-plane shear modulus of the NCF laminates.

Three different FE models have been employed in this study: the model of a single NCF lamina and the models of both a $[0,90]_2$ and a $[0,90]_s$ NCF laminate. The geometry and boundary conditions corresponding to these three models will be described in detail in the following sections.

3.1.- Finite element model of a single NCF lamina

The 3D FE model developed to evaluate the apparent stiffness of a single lamina corresponds to the minimum unit cell that, repeated through its plane, is able to generate a complete NCF lamina with parallel tows. As can be seen in Fig. 2(a), the unit cell contains two half tows and the resin pocket left between them. In the figure, the dark colour symbolizes the tows and the white colour represents the resin. To help in the understanding of the model, the resin has been taken away in Fig. 2(b) so the size, orientation and crimp of the tows can be clearly observed.

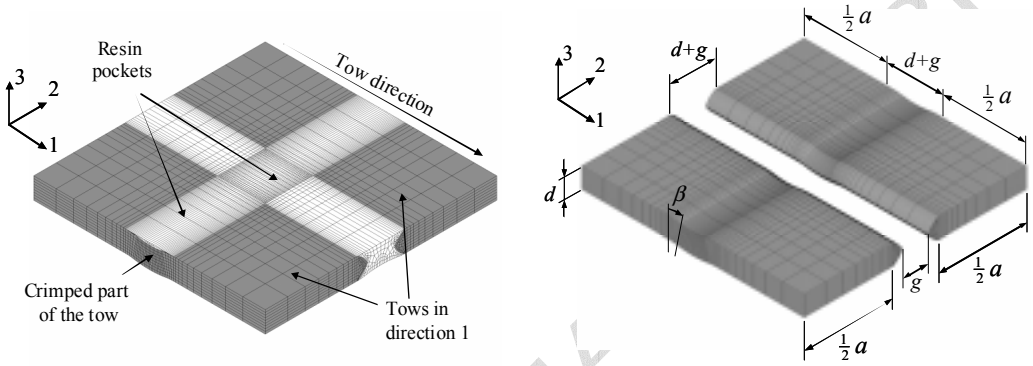

(a) (b)

Figure 2: FE model of a single NCF lamina: (a) complete model, (b) tow shape and dimensions employed for the parametric analysis.

As has been mentioned already, one of the objectives of the numerical analysis carried out is to study the influence of certain material parameters on its apparent stiffness. In this way, the geometry has been defined in a parametric way, which has made the task of developing the FE model significantly more difficult. The geometrical parameters employed are shown in Fig. 2(b), where a represents the length of the tow not affected by the crimp (which is equal to the straight part of the cross-section of the tow), d is the thickness of the lamina, g is the minimum width of the gap left between two adjacent tows of the lamina, and β is an angular parameter that represents the maximum crimp of the tows.

The FE code used has been ANSYS, and a linear solid element (SOLID45), with eight nodes and three degrees of freedom at each node, has been employed [11]. As an indication, the model shown in Fig. 2(a) contains 25280 elements and 27469 nodes.

In order to carry out a proper validation of the results obtained with those FE models, they have been made using the actual sizes and mechanical properties of the panels manufactured within the FALCOM project [12-15].

The averaged fibre volume fraction of the lamina, V_f^l, is a function of the averaged fibre volume fraction of the tows, V_f^t, and the relative sizes of the cross-section of the tow, A^t, and the cross-section of the lamina, A^l. Therefore, assuming that the two sides of the cross-section of the tow are semicircular, V_f^t and V_f^l are related by the following equation:

$$V_f^l = V_f^t \frac{A^t}{A^l} = V_f^t \frac{ad + \frac{1}{4}\pi d^2}{(a+d+g)d} \tag{5}$$

The actual values considered for parameters a, d, g and V_f^t are shown in Table 1, for the three different values of the lamina fibre content, $V_f^l = 40\%$, 50% and 60%, considered in this study. The values of the fibre volume fraction of the tows, obtained using (5), are in good agreement with the measurements shown in [12-13] (for $V_f^l = 50\%$ and 60%), since the values of parameters a, d, g and V_f^t are in good agreement too.

V_f^l (%)	V_f^t (%)	a (mm)	d (mm)	g (mm)
40	47	1.92	0.391	0.3
50	58	1.99	0.314	0.3
60	70	2.06	0.238	0.3

Table 1. Values considered for parameters a, d, g and V_f^t in the models.

As the crimp angle affecting the tows fluctuates within the laminate, several crimp values (in the range $3º < \beta < 15º$) have been considered in this study in order to analyze its influence in the global stiffness properties of the laminates.

3.2.- Finite element model of a $[0,90]_2$ NCF laminate

The FE model used to determine the stiffness properties of a $[0,90]_2$ laminate has been made by stacking four lamina models like the one described in the previous section, employing the appropriate orientation

in each lamina, as can be appreciated in Fig. 3, where the laminate model, with and without resin, is shown. Again, the dark colour symbolizes the tows and the white colour represents the resin.

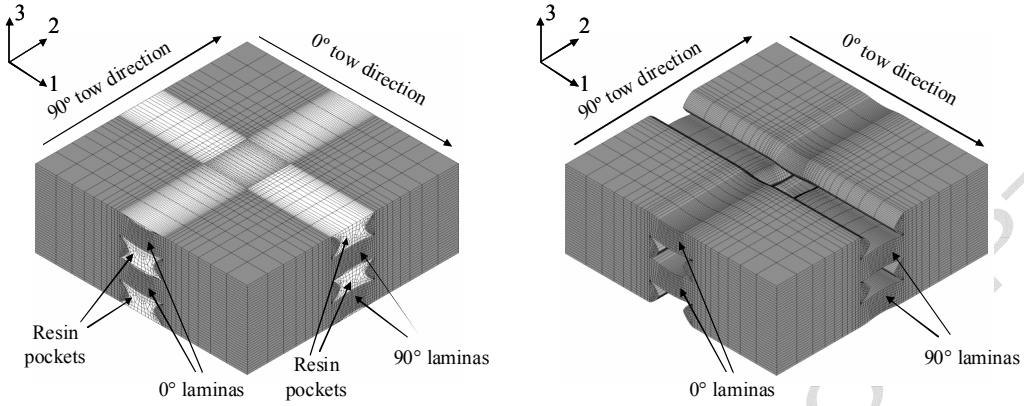

Figure 3: FE model of a $[0,90]_2$ NCF laminate: (a) complete model, (b) tow shape and orientations.

The first and third laminas of the model (starting from the top) correspond to the 0º laminas, with their tows oriented along direction 1, while the second and fourth represent the 90º laminas.

Constructing the model in this way implies that the tows of all laminas inside the laminate are not shifted in the in-plane directions, that is, the tows of equally oriented laminas are placed exactly one below the other, and the same applies to the crimped part of them. Obviously, including the real shift of the tows and its crimp between the layers would lead to a larger representative volume in the laminate and a higher complexity in the FE models.

It also has to be mentioned that several options for the crimp orientation, i.e upward crimp or downward crimp, have been considered in both the 0º and the 90º laminas, with no significant differences in the results obtained.

3.3.- Finite element model of a $[0,90]_s$ NCF laminate

The FE model developed to evaluate the stiffness properties of a $[0,90]_s$ NCF laminate has been obtained isolating the upper half of the FE model of a $[0,90]_2$ NCF, shown in Fig. 3. The upper lamina of this model represents the top 0º laminas of the laminate, and the lower lamina represents the adjacent 90º laminas of the laminate. Symmetry conditions have been applied to the model, throughout the bottom

horizontal face of the 90º lamina, in order to avoid the modelling of the two opposite laminas of the symmetric laminate.

3.4.- Boundary conditions

The procedure used to evaluate the stiffness properties of a single NCF lamina consists of applying a set of displacement boundary conditions to the model which allow the terms of the stiffness matrix of the lamina, i.e. the matrix $\boldsymbol{Q}^{0^\circ}$, to be determined. The stiffness equation of a single composite lamina is shown in (1), along with the terms of the stiffness matrix that must be evaluated in order to determine the apparent in-plane elasticity moduli, E_{11} and E_{22}, the apparent in-plane Poisson ratio ν_{12} and the apparent in-plane shear modulus G_{12} of a single NCF lamina, employing the equations shown in (2)-(4).

In order to determine the first row of the stiffness matrix, i.e. $Q_{11}^{0^\circ}$ and $Q_{12}^{0^\circ}$, the following displacements have been prescribed in the four lateral faces of the single NCF lamina model:

$$u_1 = \varepsilon_{11} x_1 \, , u_2 = 0 \, , \text{ with } \varepsilon_{11} > 0 \tag{6}$$

Likewise, in order to determine the components of the second row of the stiffness matrix, i.e. $Q_{12}^{0^\circ}$ and $Q_{22}^{0^\circ}$, the following displacements have been prescribed in the four lateral faces of the single NCF lamina model:

$$u_1 = 0 \, , u_2 = \varepsilon_{22} x_2 \, , \text{ with } \varepsilon_{22} > 0 \tag{7}$$

Finally, the boundary conditions:

$$u_1 = \gamma_{12} x_2 \, , u_2 = \gamma_{12} x_1 \, , \text{ with } \gamma_{12} > 0 \tag{8}$$

are used to impose a pure shear strain state on the single NCF lamina model, which allows the value of the term $Q_{66}^{0^\circ}$ to be evaluated.

The methodology used to evaluate the apparent stiffness properties of both a $[0,90]_2$ and a $[0,90]_s$ NCF laminate from the 3D FE models, described respectively in sections 3.2 and 3.3, is similar to the procedure used to calculate the stiffness properties of a single NCF lamina from the model described in section 3.1. In this way, firstly, a set of displacement boundary conditions is applied to the models in order to calculate the apparent stiffness matrix of the laminate and, secondly, the apparent in-plane

stiffness properties are determined using (4). The displacement fields applied correspond to those defined in (6)-(8).

Several boundary conditions have been applied in the top and bottom faces of the NCF lamina and laminates, including coupling of nodes, with no significant differences in the results obtained. The results shown in the following have been obtained with the simplest boundary conditions, i.e. traction free top and bottom faces. As has been already mentioned, in the model of a $[0,90]_s$ only two layers have been included in the model and thus symmetry boundary conditions have been applied at the bottom surface of the model (which represents the middle plane of the laminate).

4.- Stiffness properties of the constituents

The NCF composites used within the FALCOM project are constituted by an isotropic non-linear elastic matrix and transversely isotropic linear elastic carbon fibres. For low stresses, the resin employed is characterized by a tensile modulus $E^m = 3.50\,\text{GPa}$ and a Poisson's ratio $\nu^m = 0.42$, no information being available for the actual non-linear behaviour of this particular resin at high stresses. As the resin is isotropic, for low stresses its shear modulus, $G^m = 1.23\,\text{GPa}$, can be obtained from the previous properties.

Transversely isotropic carbon fibres are characterized by identical stiffness properties in all planes containing the fibre axis (with elastic constants: $E_L^f = 237\,GPa$, $\nu_L^f = 0.25$ and $G_L^f = 94.8\,\text{GPa}$) and a different isotropic behaviour in the plane normal to the fibre axis (with elastic constants: E_T^f, ν_T^f and G_T^f).

Since the FE models of the NCF laminates have been made at mesoscopic scale, the properties required to carry out the FE analysis are the stiffness properties of the resin pockets and the tows. As the tows are constituted by a large number of parallel fibres, evenly distributed and impregnated by the resin, their elastic behaviour will be transversely isotropic (with elastic constants: E_L^t, ν_L^t, G_L^t, E_T^t, ν_T^t and G_T^t). As no experimental measurement of the elastic properties of the tows has been carried out within the FALCOM project, averaging techniques have been employed to estimate their actual value as a function of the elastic properties of the constituents and the fibre and matrix volume fraction of the tow.

Three different averaging techniques have been employed: the Rule of Mixtures (RM), the Halpin-Tsai (HT) equations [16], and the Huang (H) equations [17], which result in the averaged properties shown in Table 2. Details of the estimation of each particular property with all methods are given in the Appendix.

Property	Rule of Mixtures	Halpin-Tsai	Huang
E_L^t (GPa)	167	167	167
ν_L^t	0.301	0.301	0.301
G_L^t (GPa)	4.11	9.15	4.83
E_T^t (GPa)	11.67	11.66	9.47
ν_T^t	0.420	0.136	0.311
G_T^t (GPa)	4.11	5.13	3.61

Table 2. Stiffness properties of the tows obtained with the different averaging techniques considered, for $V_f^t = 70\%$ ($V_f^t = 60\%$).

Since the apparent mechanical properties of the tows are influenced by their curvature, each tow has been developed extruding its cross-section along a line that follows the curvature of the tow. Consequently, the local coordinate systems of the finite elements modelling the tows are also oriented following this curvature. The effect of the curvature of the tows has been taken into account employing in each element its local coordinate system to define the corresponding stiffness properties.

As the behaviour of the resin at high stresses is non-linear, in reality both the tows and the resin pockets will behave non-linearly under shear, at least partially. As most of the resin of the laminate is impregnating the fibres within the tows, the non-linearity of the material behaviour of the resin pockets has a low influence in the overall non-linear elastic shear behaviour of the NCF laminate. Bearing this in mind, the resin pockets have been modelled as a linear elastic material, since the removal of this non-linearity from the model improves the convergence of the solution. Therefore, the only material non-linearity that has been taken into account in the numerical analysis is the non-linear elastic shear behaviour of the tows in the longitudinal planes (G_L^t). Details on how this non-linear material behaviour has been included in the model and its influence on the results will be shown in section 6.3.

5.- Comparison of the results obtained following the lamina and laminate procedures

In this section, the in-plane stiffness properties of several $[0,90]_2$ and $[0,90]_s$ NCF laminates, obtained using a 3D FE model of a representative unit cell of a single NCF lamina (LaNM), will be compared with the results obtained using a 3D FE model of a representative unit cell of the full laminates (LeNM).

The apparent in-plane stiffness properties calculated for a $[0,90]_2$ NCF laminate, with a fibre content $V_f^l = 60\%$ and a maximum crimp angle $\beta = 3^o$, are shown in Table 3. For each procedure (LaNM and LeNM), the apparent stiffness properties of the tows (E_L^t, E_T^t, ν_L^t, ν_T^t, G_L^t and G_T^t) have been estimated in three different ways, combining the abovementioned averaging techniques.

Lay-up - Procedure	Tow properties	$E_{11} = E_{22}$ (GPa)	ν_{12}	G_{12} (GPa)
$[0,90]_2$ - LaNM	$E_L^{t,RM}, E_T^{t,RM}, \nu_L^{RM}, \nu_T^{t,RM}, G_L^{t,RM}, G_T^{t,RM}$	76.0	0.0404	3.55
	$E_L^{t,RM}, E_T^{t,RM}, \nu_L^{RM}, \nu_T^{t,RM}, G_L^{t,HT}, G_T^{t,RM}$	76.7	0.0413	7.31
	$E_L^{t,H}, E_T^{t,H}, \nu_L^{H}, \nu_T^{t,H}, G_L^{t,H}, G_T^{t,H}$	75.5	0.0349	4.13
$[0,90]_2$ - LeNM	$E_L^{t,RM}, E_T^{t,RM}, \nu_L^{RM}, \nu_T^{t,RM}, G_L^{t,RM}, G_T^{t,RM}$	76.8	0.0427	3.86
	$E_L^{t,RM}, E_T^{t,RM}, \nu_L^{RM}, \nu_T^{t,RM}, G_L^{t,HT}, G_T^{t,RM}$	77.0	0.0435	8.33
	$E_L^{t,H}, E_T^{t,H}, \nu_L^{H}, \nu_T^{t,H}, G_L^{t,H}, G_T^{t,H}$	75.8	0.0360	4.52

Table 3. Apparent in-plane stiffness properties of a $[0,90]_2$ NCF laminate with $V_f^l = 60\%$ and $\beta = 3^o$, employing different averaging techniques to evaluate the stiffness properties.

As can be seen in the table, the stiffness properties evaluated with LaNM and LeNM procedures are quite similar and a very slight discrepancy is obtained in the apparent elasticity moduli and the Poisson ratio calculated using different averaging techniques. In contrast, a more significant influence of the averaging technique is found in the calculation of the shear modulus, this being a consequence of the lack of agreement of G_L^t estimated by the three techniques mentioned, as shown in Table 2. In the following the stiffness properties of the tows will be estimated using the Rule of Mixtures, since this is the method most commonly used.

To check that there is no influence of the stacking sequence of the NCF layers on the in-plane apparent stiffness properties, and consequently to evaluate the soundness of the LaNM procedure, a $[0,90]_2$ and a $[0,90]_s$ NCF laminate have been studied with the LeNM procedure, using the 3D FE models described in

section 3. In both cases, the laminates have a fibre volume fraction $V_f^l = 60\%$ and maximum crimp angle $\beta = 3^o$, and the tow properties have been estimated using the Rule of Mixtures. The results obtained in both models, along with the solution obtained with the LaNM procedure, are shown in Table 4, where it can be appreciated that the in-plane apparent stiffness properties predicted for both laminates are very similar. Therefore it is confirmed that, as in traditional unidirectional laminates and in accordance with the numerical predictions obtained, the stacking sequence is a parameter which does not affect the apparent in-plane stiffness properties of the laminates.

Model	Lay-up	$E_{11} = E_{22}$ (GPa)	ν_{12}	G_{12} (GPa)
LaNM	$[0,90]_2$ - $[0,90]_s$	76.0	0.0404	3.55
LeNM	$[0,90]_2$	76.8	0.0427	3.86
	$[0,90]_s$	76.8	0.0427	3.86

Table 4. Apparent in-plane stiffness properties of a $[0,90]_2$ and a $[0,90]_2$ NCF laminate with a fibre content $V_f^l = 60\%$ and a maximum crimp angle $\beta = 3^o$, employing different FE models.

With the analyses carried out, the good agreement between the apparent stiffness of a $[0,90]_2$ and a $[0,90]_s$ NCF laminate, calculated with both methods described in section 2, has been shown. Therefore, it can be concluded that the calculation of the stiffness properties of NCF laminates from the in-plane apparent stiffness properties of their laminas, applying the General Laminate Theory, can be a valid alternative method to evaluate the stiffness properties of NCF laminates, avoiding the need to model the whole thickness of the laminate. Consequently a high reduction in the complexity of the FE models is obtained, especially when laminas are oriented in directions other than 0º and 90º.

6.- Parameters affecting the apparent stiffness properties

In the following sections, the influence that the different parameters defining the internal geometry may have in the apparent in-plane stiffness properties of the NCF laminates is presented. Once the equivalence between the LaNM and LeMN procedures has been stated, any of them can be used for the subsequent analyses. The LaNM procedure will be employed in sections 6.1 and 6.2 to study, respectively, the influence of the maximum crimp angle in the tows, β, and the fibre volume fraction of the laminate, V_f^l,

in the apparent stiffness properties of several $[0,90]_s$ NCF laminates. In section 6.3 the influence of the non-linear shear behaviour of the tows will be analyzed using the LeNM procedure.

6.1.- Maximum crimp angle

As is well known, the mechanical properties of the composite materials decrease with the curvature of the fibres. Despite their name, fibres in the NCF laminates are slightly crimped as a consequence of their internal structure (based on tows) and the manufacturing techniques employed. In this section, the apparent in-plane stiffness properties of a $[0,90]_s$ NCF laminate, with a fibre volume fraction $V_f^l = 60\%$, are evaluated as a function of the increasing crimp angle of the tows in the range $0º < \beta < 15º$. In all these models, the averaged stiffness properties of the tows have been estimated using the Rule of Mixtures.

The numerical results obtained for the apparent in-plane stiffness properties of a $[0,90]_s$ NCF laminate, calculated using the LaNM procedure, are shown in Table 5 as a function of the maximum crimp angle β defined in Fig 2(b).

β	$E_{11} = E_{22}$ (GPa)	ν_{12}	G_{12} (GPa)
0º	77.9	0.0404	3.88
3º	76.0	0.0404	3.55
6º	74.7	0.0407	3.58
9º	72.4	0.0410	3.58
12º	69.7	0.0415	3.58
15º	67.4	0.0427	3.56

Table 5. Apparent in-plane stiffness properties of a $[0,90]_s$ NCF laminate with $V_f^l = 60\%$ and different crimp angles (β).

In view of the results, the following conclusions are obtained: when the crimp angle increases from $\beta = 0º$ to $\beta = 15º$, the tensile modulus $E_{11} = E_{22}$ decreases roughly linearly, the maximum decrease being 13.5%. Poisson ratio increases slightly, and again almost linearly, but it is less influenced by the tow crimp, the maximum increase being 5.7%. Finally, the shear modulus is reduced by 8.0% as a result of tow crimp, this reduction being nearly independent of the crimp angle. Although the influence shown is not dramatic, its clear that reducing to a minimum the crimp angle in an NCF laminate should be a principal objective of a production technique in order to obtain higher stiffness properties.

6.2.- Fibre volume fraction

In this section, three different values of the fibre volume fraction of the laminates ($V_f^l = 40\%$, 50% and 60%) have been considered in the numerical analysis of the apparent in-plane stiffness properties of a $[0,90]_s$ NCF laminate. Following the experimental measurements carried out in actual NCF laminates, the variation of the fibre content of the laminate implies a variation of the fibre volume fraction of the tows and of the dimensions defining the internal architecture of the material. Both features have been taken into account in the model, as shown in Table 1. In all these models, the averaged stiffness properties of the tows have been estimated using the Rule of Mixtures with a maximum crimp angle $\beta = 3^o$.

The numerical results, calculated using the LaNM procedure, obtained for the apparent in-plane stiffness properties of a $[0,90]_s$ laminate, as a function of the fibre content, are shown in Table 6. As can be observed, an increase in the fibre content from $V_f^l = 40\%$ to $V_f^l = 60\%$, results in a roughly linear increase in the elasticity modulus by 34% and in the shear modulus by 37%, while the Poisson ratio remains almost constant.

Method	Property	Fibre content (V_f^l)		
		40%	50%	60%
LaNM	$E_{11} = E_{22}$ (GPa)	50.2	62.3	76.0
	ν_{12}	0.0430	0.0400	0.0404
	G_{12} (GPa)	2.23	2.79	3.55
Rule of Mixtures	$E_{11} = E_{22}$ (GPa)	51.8	63.9	76.6
	ν_{12}	0.0399	0.0369	0.0365
	G_{12} (GPa)	2.06	2.46	3.08

Table 6. Apparent stiffness properties of a $[0,90]_s$ NCF laminate and different fibre contents (V_f^l) calculated by the LaNM (with $\beta = 3^o$) and the Rule of Mixtures.

The comparison of these numerical results, corresponding to a crimp angle $\beta = 3^o$, with the estimation obtained by a direct application of the Rule of Mixtures (which does not take crimp into account) is also interesting. The results included in Table 6 show that the variation described above for the numerical results is quite similar to the variation observed in the results obtained after the direct application of the

Rule of Mixtures. However, even for the very low crimp angle employed in this analysis, some differences are found in the results shown in Table 6. If compared with the LaNM predictions, the Rule of Mixtures overestimates slightly the tensile modulus, the differences being larger for low fibre volume fractions, while the opposite applies for the shear modulus, which is slightly underestimated by the Rule of Mixtures, the differences being larger for high fibre volume fractions.

These discrepancies increase for higher crimp angles as can be seen comparing the predictions of the Rule of Mixtures shown in Table 6 with the numerical predictions shown in Table 5, for $V_f^l = 60\%$.

6.3.- Non-linear shear behaviour of the tows

As was previously discussed in section 4, the tows in the NCF laminates behave as a transversely isotropic non-linear elastic material, while the resin behaves as an isotropic non-linear elastic material. Due to the limitations in the analysis code, the non-linear transversely isotropic material behaviour of the tows has been modelled as a bilinear anisotropic material behaviour. In fact, using a co-ordinate system with direction X oriented tangentially to the fibre axis and directions Y and Z contained in the cross section plane, the only non-linearity is an equal bilinear relationship between the pairs $\sigma_{xy} / \gamma_{xy}$ and $\sigma_{xz} / \gamma_{xz}$. For the sake of simplicity, in the following, both shear behaviours in the longitudinal planes of the tows will be referred to as τ_L^t / γ_L^t.

The first slope of the τ_L^t / γ_L^t bilinear relationship ($G_L^{t,I} = 4.11\text{GPa}$) has been evaluated from the stiffness properties of its constituents, using the Rule of Mixtures. As no information was available about the non-linear behaviour of the resins considered within the FALCOM project, several values of the second slope of the τ_L^t / γ_L^t bilinear relationship ($G_L^{t,II}$) have been considered in order to analyze its influence in the apparent stiffness of the laminate.

A $[0,90]_2$ NCF laminate, with a fibre content $V_f^l = 60\%$ and a maximum crimp angle $\beta = 3^o$, has been chosen for the analysis, using the LeNM procedure with the boundary conditions described in (6)-(8), corresponding to average strain states in which only one of the in-plane strains is not null. Therefore, an average $\varepsilon_{11} > 0$ (with $\varepsilon_{22} = \gamma_{12} = 0$) will be applied to study E_{11} and ν_{12}, and an average $\gamma_{12} > 0$ (with $\varepsilon_{11} = \varepsilon_{22} = 0$) to study G_{12}. In the laminate under consideration, E_{22} is identical to E_{11}.

In this section, a value of $G_L^{t,II} = 0.75\,\text{GPa}$ has been chosen for the second slope of the τ_L^t / γ_L^t bilinear relationship, and the change in slope has been introduced in each element when either σ_{xy} or σ_{xz} reaches the value $\tau_L^{t,*} = 60\,\text{GPa}$. The results obtained with different values of $G_L^{t,II}$ will be shown in the next section compared with the experimental measurements corresponding to actual NCF coupons.

As expected, the in-plane tensile moduli E_{11} and the in-plane Poisson ratio ν_{12} of the laminates are not influenced by the non-linear shear behaviour of the tows. This can be clearly appreciated in Fig. 4, where the E_{11} / E_{11}^0 and ν_{12} / ν_{12}^0 ratios are plotted against the corresponding averaged applied strains. In this plot, E_{11} and ν_{12} are the apparent stiffness properties for a certain value of the corresponding applied strain (secant stiffness properties), while E_{11}^0 and ν_{12}^0 are the initial tangent stiffness properties. Therefore, by definition, $E_{11} \to E_{11}^0$ and $\nu_{12} \to \nu_{12}^0$ when $\varepsilon_{11} \to 0$.

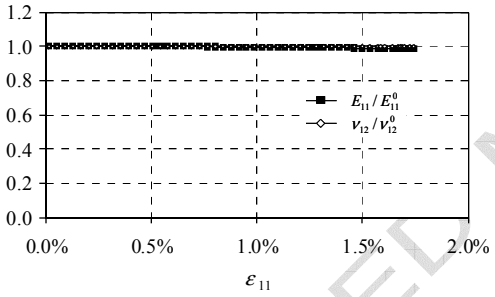

Figure 4: E_{11} / E_{11}^0 and ν_{12} / ν_{12}^0 ratios versus the averaged applied strain (ε_{11}) in a $[0,90]_2$ NCF laminate.

On the other hand, from the results of the analysis it can be observed that the apparent shear modulus of the laminates, G_{12}, is clearly influenced by the non-linear shear behaviour of the tows. In fact, as can be appreciated in Fig. 5, where the averaged shear stress σ_{12} is plotted versus the averaged applied strain γ_{12}, the averaged in-plane shear behaviour of the NCF laminate ($\sigma_{12} / \gamma_{12}$) reproduces the bilinear shear behaviour of the tows in the longitudinal planes (τ_L^t / γ_L^t).

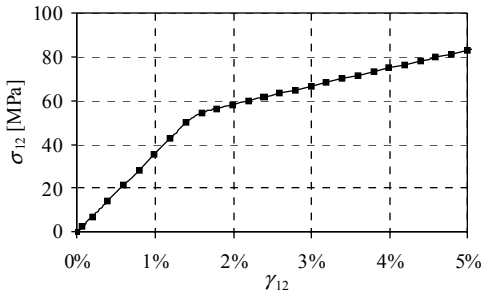

Figure 5: Averaged in-plane shear stress σ_{12} versus averaged applied strain (γ_{12}) in a $[0,90]_a$ NCF laminate.

Finally, the shear modulus G_{12}/G_{12}^0 ratio is plotted in Fig. 6 versus the averaged applied shear strain γ_{12}. In this plot, G_{12} is the instantaneous apparent in-plane shear modulus (secant modulus), while G_{12}^0 is the initial tangent in-plane shear modulus. As can be seen, after an initial plateau, in which G_{12} is equal to G_{12}^0, the secant modulus G_{12} decreases steadily. This decrease in G_{12} is associated with the increase in size of the zone of the tows in which the second slope of the bilinear shear behaviour has been reached.

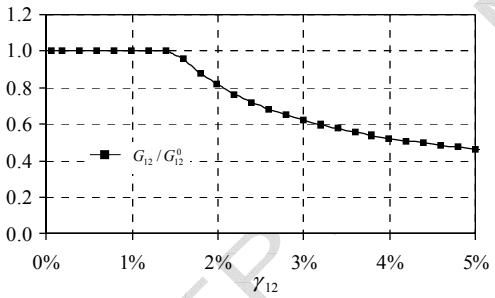

Figure 6: G_{12}/G_{12}^0 ratio versus the averaged applied strain (γ_{12}) in a [0,90, 0,90] NCF laminate.

7.- Comparison with coupon data

A series of experimental stiffness measurements have been carried out by different partners within the FALCOM Project, corresponding to NCF laminates, with different lay-ups, fibre volume fractions and manufacturing techniques. In this paper, and for the purpose of validation, the case corresponding to a $[0,90]_2$ NCF laminate with a fibre volume fraction $V_f^t = 60\%$ manufactured by resin film infusion has

been selected due to the fact that it has been the most tested case (being defined in the FALCOM Project as the Benchmark problem) and also numerically the case studied in the greatest depth.

Of course, the material properties employed for the numerical analysis presented in the previous sections (described in section 3.2) correspond to the actual material properties of the resin and fibres employed in the manufacturing of the samples.

In fact, the actual tested $[0,90]_2$ NCF samples have been cut from $[+45,-45]_2$ plates in two orthogonal orientations (warp and weft), both resulting sets of samples having slightly different mechanical properties, although ideally all samples should have been identical.

As has already been established, the apparent in-plane tensile moduli, E_{11} and E_{22}, and the apparent in-plane Poisson ratio, ν_{12}, present a linear behaviour, while the apparent shear modulus, G_{12}, is clearly non-linear. Therefore, these properties will be treated separately. For the laminate chosen there is no distinction between E_{11} and E_{22}, and both will be denoted by E in this section.

The experimental results [14-15] for the apparent in-plane elasticity modulus, E, the apparent in-plane Poisson ratio, ν_{12}, and the apparent in-plane shear modulus, G_{12}, (corresponding to the initial linear slope) are shown in Table 7. As can be seen, there is a certain scatter in the experimental results and some differences are found between the results corresponding to the differently oriented samples, particularly for ν_{12}. Therefore, these values should be taken as typical values.

Orientation	E (GPa) [CoV]	ν_{12} [CoV]	G_{12} (GPa) [CoV]
Warp	70.1 [2.7%]	0.042 [33.7%]	4.85 [2.2%]
Weft	71.2 [1.8%]	0.044 [9.6%]	5.31 [4.2%]

Table 7. Experimental measurements of the apparent in-plane stiffness properties of a [0,90, 0,90] NCF laminate.

Nevertheless, if the experimental results are compared with the numerical predictions shown in Table 5, a fairly good agreement is found between the experimentally measured in-plane stiffness properties and the predictions made for a maximum crimp angle of $\beta = 12^{\circ}$. This value of the crimp angle was found to be

in the order of a reasonable average creep angle of the material employed. For this particular crimp value of $\beta = 12^{o}$, the numerical predictions for the apparent in-plane elasticity modulus, E, and the apparent in-plane Poisson ratio, ν_{12}, are very close to the average experimental values, the difference being lower than the scatter of the experimental measurements.

As expected, the most significant discrepancies between the experimental results and the numerical predictions are found in the apparent in-plane shear stiffness, G_{12}. This can be due to several reasons: lack of information about the actual non-linear behaviour of the resin, disagreement between the different averaging techniques employed to obtain the stiffness properties of the tows, idealised bilinear shear behaviour of the tows, and discrepancies between the experimental results corresponding to differently oriented samples. However, if two typical experimentally measured $\sigma_{12} / \gamma_{12}$ non-linear relationships (corresponding to the warp and weft orientations) are plotted together with three different numerical simulations (corresponding to different values of the second slope, $G_L^{t,II}$, of the bilinear shear behaviour of the tows in the longitudinal planes), the results shown in Fig. 7 are obtained.

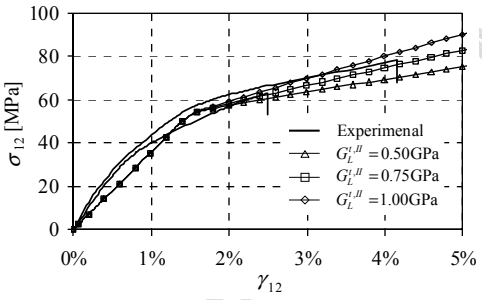

Figure 7: Experimental measurements and numerical predictions for the apparent $\sigma_{12} / \gamma_{12}$ non-linear relationship for a $[0,90]_2$ NCF laminate.

As can be seen, a reasonably good agreement is found in the overall shear behaviour in all cases, and the major differences seem to be due to the idealised bilinear shear behaviour of the tows.

8.- Concluding remarks

NCF composites are characterized by a complicated internal microstructure that makes it difficult to elucidate whether the traditional rules employed to predict the stiffness of tape based composites are valid for this kind of composite material. For this reason, several 3D FE models of the representative unit cell

of a single NCF lamina and some NCF laminates have been developed to evaluate numerically the apparent in-plane stiffness properties of NCF laminates.

The first conclusion that can be extracted from the numerical analyses carried out is that the application of the General Laminate Theory to obtain the apparent in-plane stiffness properties of an NCF laminate is valid for this material, once the particular characteristics of its microstructure have been taken into account to obtain the properties of the laminas. The use of this approach will be particularly interesting when dealing with laminates which have orientations different to 0º and 90º, in which the building of a through thickness 3D FE model is extraordinarily complicated.

To validate the results obtained with the above-mentioned models, numerically predicted apparent in-plane stiffness of a $[0,90]_2$ NCF laminate has been successfully compared with experimental measurements carried out within the FALCOM project.

Therefore, using these 3D FE models, numerical predictions for the influence of the maximum crimp angle in the tows, the fibre volume fraction of the laminate and the non-linear shear behaviour of the tows in the apparent in-plane stiffness properties of a $[0,90]_s$ NCF laminate have been presented.

It has been shown that the main effect of the crimp of the tows is a reduction in the tensile modulus, which is roughly proportional to the maximum crimp angle. If the crimp angle is maintained constant, the dependency of the stiffness properties upon the fibre volume fraction obtained with the numerical models is similar to the dependency obtained in traditional composites. Finally, the numerical results show that the use of a simple appropriate bilinear shear behaviour of the tows permits a fairly good prediction of the non-linear shear behaviour of the NCF laminate to be obtained.

Acknowledgements

This work has been financed in part by the European Commission's support of the project FALCOM (Failure, Performance and Processing Prediction for Enhanced Design with Non-Crimp-Fabric Composites) under EC contract No. G4RD-CT-00694.

The authors gratefully acknowledge F. Edgren, L.E. Asp and R. Joffe for permitting the reproduction of their micrograph of the cross-section of a typical NCF composite.

Appendix

The apparent stiffness properties of the tows in the longitudinal planes (E_L^t, ν_L^t and G_L^t) and the transverse planes (E_T^t, ν_T^t, and G_T^t) have been estimated from the resin stiffness properties (E^m, ν^m and G^m) and the stiffness properties of the fibres in the longitudinal (E_L^f, ν_L^f and G_L^f) and transverse (E_T^f, ν_T^f and G_T^f) planes, using three different interpolation techniques: the Rule of Mixtures (RM), the Halpin-Tsai (HT) equations [16], and the Huang (H) equations [17].

In the three approaches, the longitudinal elasticity modulus, E_L^t, and Poisson's ratio, ν_L^t, are interpolated identically using the following expressions:

$$\begin{aligned} E_L^{t,RM} &= E_L^{t,HT} = E_L^{t,H} = E_L^f V_f^t + E^m V_m^t \\ \nu_L^{t,RM} &= \nu_L^{t,HT} = \nu_L^{t,H} = \nu_L^f V_f^t + \nu^m V_m^t \end{aligned} \tag{9}$$

In contrast, the evaluation of the longitudinal shear modulus, G_L^t, and the transverse elasticity modulus, E_T^t, and shear modulus, G_T^t, has different interpolations depending on the approach employed.

Thus, using the Rule of Mixtures, taking into account that the fibre is much stiffer than the matrix, the following interpolation rules have been employed:

$$E_T^{t,RM} \approx E^m / V_m^t \;,\quad G_T^{t,RM} \approx G^m / V_m^t \;,\quad G_L^{t,RM} = G^m / V_m^t \tag{10}$$

with, V_f^t and V_m^t being, respectively, the fibre and matrix volume fraction in the tow.

Using the Halpin-Tsai equations, the following interpolation rules have been employed:

$$\begin{aligned} E_T^{t,HT} &= E^m (1+\xi_T^E \eta_T^E V_f^t)/(1-\eta_T^E V_f^t) \\ G_T^{t,HT} &= G^m (1+\xi_T^G \eta_T^G V_f^t)/(1-\eta_T^G V_f^t) \\ G_L^{t,HT} &= G^m (1+\xi_L^G \eta_L^G V_f^t)/(1-\eta_L^G V_f^t) \end{aligned} \tag{11}$$

with

$$\begin{aligned} &\xi_T^E = 2+40(V_f^t)^{10} \;,\; \eta_T^E = [(E_L^f / E^m)-1]/[(E_L^f / E_L^f)+\xi_T^E] \\ &\xi_T^G = [4-3\nu^m]^{-1} \;,\; \eta_T^G = [(V_f^t / V_m^t)-1]/[(V_f^t / V_m^t)+\xi_T^G] \\ &\xi_L^G = 1+40(V_f^t)^{10} \;,\; \eta_L^G = [(G_L^f / G^m)-1]/[(G_L^f / G^m)+\xi_L^G] \end{aligned} \tag{12}$$

And, using the Huang equations, the following interpolation rules have been employed:

$$
\begin{aligned}
E_T^{t,H} &= \frac{(V_f^t + V_m^t a_{11})(V_f^t + V_m^t a_{22})}{(V_f^t + V_m^t a_{11})(V_f^t S_{22}^f + a_{22} V_m^t S_{22}^m) + V_m^t V_f^t a_{12}(S_{21}^m - S_{21}^f)} \\
G_L^{t,H} &= G^m \frac{(G_{12}^f + G^m) + V_f^t (G_{12}^f - G^m)}{(G_{12}^f + G^m) - V_f^t (G_{12}^f - G^m)} \\
G_T^{t,H} &= \frac{0.5(V_f^t + V_m^t a_{22})}{V_f^t (S_{22}^f - S_{23}^f) + V_m^t a_{22}(S_{22}^m - S_{23}^m)}
\end{aligned}
\tag{13}
$$

where $\boldsymbol{S}^f$ and $\boldsymbol{S}^m$ are, respectively, the compliance matrices of fibre and matrix, and:

$$
a_{11} = \frac{E^m}{E_L^f},\ a_{22} = \frac{1}{2}\left(1 + \frac{E^m}{E_T^f}\right),\ a_{12} = (a_{11} - a_{22})\frac{S_{12}^f - S_{12}^m}{S_{11}^f - S_{11}^m} \tag{14}
$$

As no information is available for the actual value of E_T^f in the fibres, a typical value of $E_T^f = 15\,\text{GPa}$ has been employed. Finally, the Poisson's ratio in transverse planes has been obtained from the isotropy condition as:

$$
\nu_T^t = \frac{E_T^t}{2G_T^t} - 1 \tag{15}
$$

References

[1] Bibo GA, Hogg PJ and Kemp M. Mechanical characterisation of glass- and carbon-fibre-reinforced composites made with non-crimp fabrics. Composites Science and Technology 1997; 57:1221-1241

[2] Edgren F, Asp LE, Joffe R. Failure of NCF composites subjected to combined compression and shear loading. Composites Science and Technology 2006;66:2865-2877.

[3] Ávila R. NCF processability and performance: a literature review. DERA/MSS/MSMA2/WP003564, Farnborough, UK, 2000.

[4] Drapier S, Wisnom MR. Finite-element investigation of the compressive strength of non-crimp-fabric-based composites. Composites Science and Technology 1999;59:1287-1297.

[5] Drapier S, Wisnom MR. A finite-element investigation of the interlaminar shear behaviour of non-crimp-fabric-based composites. Composites Science and Technology 1999;59:2351-2362.

[6] París F, González A, Graciani E, Flores M, del Castillo E. A 3D FEM study of compressive behaviour of non-crimp fabrics, (paper FM7). In: Proceedings of the 11th European conference on composite materials (ECCM11), May 31–June 3, 2004, Rhodes, Greece.

[7] Edgren F, Mattsson D, Asp LE, Varna J. Formation of damage and its effects on non-crimp fabric reinforced composites loaded in tension. Composites Science and Technology 2004;64:675-692.

[8] Edgren F, Asp LE. Approximate analytical constitutive model for non-crimp fabric composites. Composites: Part A 2005;36;173-181.

[9] Joffe R, Mattsson D, Modniks J, Varna J. Compressive failure analysis of non-crimp fabric composites with large out-of-plane misalignment of fiber bundles. Composites: Part A 2005;36:1030-1046.

[10] Tessitore N, Riccio A. A novel FEM model for biaxial non-crimp fabric composite materials under tension. Computers and Structures 2006;84:1200-1207.

[11] ANSYS Release 8.0 Documentation. Swanson Analysis Systems, Inc. 2003.

[12] Mattsson D, Joffe R and Varna J. Methodology for characterization of internal structure parameters governing performance in NCF composites.Composites Part B 2007;38:44-57

[13] Mattson D, Joffe R and Varna J. Characterisation of processability and manufacturing. Characterisation of microstructure. FALCOM/WP2:D2.1-4/LTU.

[14] Joffe R. Characterization of performance. Performance in tension. Elastic properties and failure. FALCOM/WP3:T3.2.1/LTU.

[15] Joffe R. Characterization of performance. Performance in tension. In-plane shear. FALCOM/WP3:T3.2.1/LTU/IPS.

[16] Halpin JC. Primer on Composite Materials Analysis (Second Edition, Revised). Technomic Publishing, 1992.

[17] Huang ZM. Simulation of the mechanical properties of fibrous composites by the bridging micromechanics model. Composites: Part A 2001;32:143-172.